Materials Chemistry and Physics 136 (2012) 897–902

Contents lists available at SciVerse ScienceDirect

Materials Chemistry and Physics

journal homepage: www.elsevier.com/locate/matchemphys

Efficient removal of methylene blue over composite-phase $BiVO_4$ fabricated by hydrothermal control synthesis

Lili Zhang [a,b,*], Jinxin Long [a], Wenwen Pan [a], Shouyong Zhou [a], Junwu Zhu [c], Yijiang Zhao [a], Xin Wang [c], Guozhong Cao [b,**]

[a] Jiangsu Key Laboratory for Chemistry of Low-Dimensional Materials, Huaiyin Normal University, Huai'an, Jiangsu 223300, PR China
[b] Materials Science and Engineering, University of Washington, Seattle, WA 98195, USA
[c] Key Laboratory of Soft Chemistry and Functional Materials, Nanjing University of Science and Technology, Nanjing 210097, China

HIGHLIGHTS

- Hybrid-phase $BiVO_4$ with different η_{mono} was controlling synthesized by hydrothermal method.
- The hybrid-phase $BiVO_4$ takes on petal-like structure when η_{mono} reaches over 60%.
- The composite $BiVO_4$ with η_{mono} = 92.73% presents the best photocatalytic activity.
- Possible mechanism for its high efficiency was put forward.

GRAPHICAL ABSTRACT

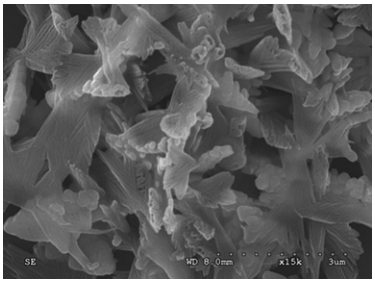

ARTICLE INFO

Article history:
Received 18 March 2012
Received in revised form
5 July 2012
Accepted 5 August 2012

Keywords:
Microstructure
Chemical synthesis
Semiconductors
Electron microscopy (STEM, TEM and SEM)

ABSTRACT

Series of composite-phase $BiVO_4$ (scheelite-tetragonal and scheelite-monoclinic) were synthesized by hydrothermal method. The mass content of monoclinic phase ($\eta_{mono} = I_{mono}/(I_{mono} + I_{tetra}) \times 100\%$) in composite-phase $BiVO_4$ was successfully controlled by adjusting the pH value of precursor solution, which was achieved by manipulating the dosage of 2 M NaOH during the synthetic reaction. Results indicated that the pH value of the precursor solution had great effect on the structure of $BiVO_4$. It took on pure tetragonal form with solid and spherical morphology when pH $\leq$ 3.8, but presented pure monoclinic structure with quadrate flake appearance when pH $\geq$ 8.5. Along with the increase of pH (3.8–8.5) and the η_{mono}, the tetragonal particles and monoclinic particulates began to link together, and the two phases interweave together to form a petal-like structure when η_{mono} reached over 60% (pH = 4.7). The photocatalytic activities of obtained products were investigated by photodegradation of methylene blue under visible light. It was found that composite-phase $BiVO_4$ with $\eta_{mono} > 60\%$ presented better photocatalytic activity than that of pure phase $BiVO_4$, either monoclinic or tetragonal. About 95% of the 10 mg L^{-1} methylene blue was degraded within 120 min catalyzed by the best catalyst $BiVO_4$ with η_{mono} = 92.73%. Possible mechanism was put forward.

1. Introduction

Energy crisis and environmental security have come to the forefront of both global and national priorities. The sustainable development of human society will depend on how to solve the urgent resources and environment issues [1,2]. Semiconductor photocatalysis is an advanced technology which can convert the

* Corresponding author. Jiangsu Key Laboratory for Chemistry of Low-Dimensional Materials, Huaiyin Normal University, Huai'an, Jiangsu 223300, PR China. Tel.: +86 517 83525083; fax: +86 517 83525369.
** Corresponding author.
E-mail address: Zhanglily800@yahoo.com.cn (L. Zhang).

0254-0584/$ – see front matter © 2012 Elsevier B.V. All rights reserved.
http://dx.doi.org/10.1016/j.matchemphys.2012.08.016

harmless and inexhaustible solar energy into chemical energy and pollutants can be removed in the presence of converting chemical energy [3–6]. If successfully developed with an economic viability, this would be the ultimate technology that could solve both energy and environmental problems altogether in the future. Early studies on photocatalysts mainly focused on the TiO_2 because of its low cost, high efficiency, and photostability [7,8]. However, TiO_2 with the band gap of 3.2 eV responds only to ultravisible (UV) light, which takes up only ca. 4% of the sunlight energy while visible-light accounts for ca. 43% [9,10]. Hereby, the development of visible-light-driven photocatalysts has now become one of the most challenging topics.

Recently, Bismuth vanadate ($BiVO_4$) has attracted increasing attention as one of the widely applied materials, a non-toxic yellow pigment, an excellent electric, magnetic materials and an effective photocatalyst for pollutant photodegradation under visible light (>420 nm) irradiation [11–15]. It was reported that there are three polymorphic forms of $BiVO_4$ [16]: zircon-tetragonal, scheelite-tetragonal, and scheelite-monoclinic. In general, the scheelite-monoclinic form of $BiVO_4$ has higher photocatalytic activity than the other two phases [17,18]. But there are quite few references about composites-phase $BiVO_4$ and its photocatalytic activity. It is well known that TiO_2 also has various phases [19], including anatase, rutile, brookite, etc. But the acknowledged TiO_2 with optimal photocatalytic activity is Degussa P25, which consists of 80% anatase and 20% rutile [20,21]. Its best photoactivity is due to a rutile sink, allowing an anatase-originating hole to move to the rutile surface and preventing anatase recombination [22]. Similarly, we speculated that the mixed-phase of $BiVO_4$ may have more efficient photoactivity than that of pure phase $BiVO_4$. Zhang et al. [23] had synthesized a series of $BiVO_4$ including pure form and hybrid-phase by hydrothermal method and they found that one of the mixed-phase $BiVO_4$ presented better photocatalytic activity. But they didn't discuss why the composite-phase $BiVO_4$ has better catalytic activity and did not study the effect of the content of monoclinic phase $BiVO_4$ on the photoactivity of mixed-phase $BiVO_4$.

In this study, we synthesized a series of composite-phase $BiVO_4$ with different contents of monoclinic $BiVO_4$ by a simple and facile route based on the hydrothermal method. Photodecomposition of methylene blue (MB) was used as the model system to investigate the photocatalytic activity of the as-prepared $BiVO_4$, and a series of high effective mixed-phase $BiVO_4$ were obtained. The possible photocatalytic mechanism of its high efficiency was studied.

2. Experimental

2.1. Materials and synthesis of bismuth vanadate

Analytical grade of Ammonium metavanadate (NH_4VO_3 99.0%) and Bismuth nitrate pentahydrate ($Bi(NO_3)_3\cdot 5H_2O$ 99.0%) supplied by Sinopharm Chemical Reagent Co., Ltd, used without any purification. Other chemicals used were all analytical grade. Solutions were prepared using deionized water. A proper amount of $Bi(NO_3)_3\cdot 5H_2O$ and NH_4VO_3 (the molar ratio of $Bi(NO_3)_3\cdot 5H_2O$:NH_4VO_3 was fixed at 1:1) was dissolved in 10 mL 2 M HNO_3 and different volume of 2 M NaOH respectively in order to control the pH values of precursor solution (shown in Table 1). In a typical preparation, 8.00 mmol of $Bi(NO_3)_3\cdot 5H_2O$ was dissolved in 10.0 mL of HNO_3 (2 M) and 8.00 mmol of NH_4VO_3 was dissolved in 17.8 mL of NaOH solution (2 M). Each solution was stirred for 0.5 h at room temperature. After that, these two mixtures were mixed together and stirred for another 2.5 h to get a salmon pink suspension with the pH value of 5.2. Then the precursor suspension was sealed in a 100 mL Teflon-lined stainless autoclave and heated at 140 °C for 6 h under autogenous pressure [24,25]. Afterward, the precipitate was filtered, washed with distilled water and absolute alcohol, and then dried in vacuum at 80 °C for 12 h.

Table 1
Volume of 2 mol L^{-1} NaOH in the synthetic section, pH values of the precursor mixture and the obtained samples were marked as $BiVO_4$-*x* (*x* = a–g).

Item	Sample						
	(a)	(b)	(c)	(d)	(e)	(f)	(g)
Volume of NaOH (mL)	17.0	17.2	17.4	17.6	17.8	18.0	18.5
pH values of precursor	3.8	4.0	4.3	4.7	5.2	5.5	8.5

2.2. Characterization

The crystalline phase structure of the as-prepared samples was determined by ARL/X/TRA X-ray diffractometer using Cu Kα radiation ($\lambda = 0.15418$ nm) in the range of 10–80° at room temperature. The BET surface area was evaluated by N_2 adsorption in a constant volume adsorption apparatus (Coulter SA 3100). The morphology was determined by scanning electron microscopy (SEM) using LEO-1530VP SEM microscopy at 25 keV. The UV–vis diffuse reflectance spectra were obtained in the range of 200–800 nm at room temperature using a UV–visible spectrophotometer (UV-1100 spectrometer).

2.3. Photodegradation experiments

Photocatalytic activities of the obtained $BiVO_4$ samples were determined by the decolorization of methylene blue (MB) using XPA photochemical reactor under visible-light irradiation of a 500-W Xe lamp with a 420 nm cutoff filter. Experiments were performed at ambient temperature as follows: First, 0.25 g of the as-prepared sample was added to 250 mL of 10 mg L^{-1} methylene blue solution with constant magnetic stirring. Before illumination, the solution was stirred for 30 min in darkness in order to reach the adsorption–desorption equilibrium. At given time intervals, 5 mL of the suspension were sampled and centrifuged to remove the photocatalytic particles from the aqueous solution so as to obtain the supernatant for the analysis of residual MB. The concentrations of MB were monitored with a UV-1100 spectrometer in terms of the absorbance at 664 nm during the photodegradation process.

3. Results and discussion

3.1. Characterization of the $BiVO_4$ powders

Fig. 1 shows the XRD patterns of the as-prepared samples at different pH values. For $BiVO_4$-a synthesized at pH = 3.8, all diffraction peaks can be assigned to the tetragonal $BiVO_4$ (JCPDS 14-0133). As the pH value increasing from 3.8 to 5.5, the peaks for the monoclinic $BiVO_4$ (JCPDS 14-0688) began to appear and the characteristic peak (121) corresponding to monoclinic $BiVO_4$ became stronger and stronger, whereas the typical peak (200) relating to tetragonal phase decreased gradually (Fig. 1b–f), indicating mixed phase of monoclinic and tetragonal $BiVO_4$ formed. As the pH increases to 8.5 (Fig. 1g), all diffractions peaks of the $BiVO_4$ can be assigned to the pure monoclinic $BiVO_4$. The results suggested that the pH value of the precursor solution is an important factor in preparing different phases of $BiVO_4$. The main reason of this phenomenon can be interpreted by the relevant chemical reactions following the synthesis route [26]

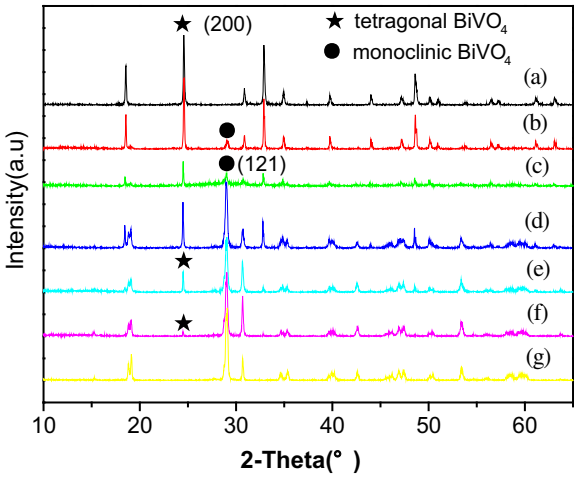

Fig. 1. XRD patterns of $BiVO_4$ synthesized at different pHs (a) pH = 3.8, (b) pH = 4.0, (c) pH = 4.3, (d) pH = 4.7, (e) pH = 5.2, (f) pH = 5.5, (g) pH = 8.5. The dark circles and stars indicate the peaks representing the monoclinic (121) and tetragonal (200) forms of $BiVO_4$, respectively.

$$Bi(NO_3)_3 + H_2O \Leftrightarrow 2HNO_3 + BiONO_3 \quad (a)$$

$$BiONO_3 + VO_4^- \Leftrightarrow BiVO_4 + NO_3^- \quad (b)$$

From equation (a), with the increase of the pH value of the precursor solution, the concentration of HNO_3 decreases, which can promote the production of $BiONO_3$ and then lead to the nucleation of $BiVO_4$ (equation b) [14]. So the formation speed of $BiONO_3$ might be the key role in the producing $BiVO_4$ nucleus. When pH = 3.8, the concentration of $BiONO_3$ is low, and leads to a slow nucleation of $BiVO_4$. Under this condition, nucleation rate of $BiVO_4$ is slower than its growth rate and $BiVO_4$ nucleus tends to heterogeneous nucleation, which is benefit to the formation of tetragonal phase. Whereas in basic solution, the nucleation rate of $BiVO_4$ nuclei might be higher than its growth rate, which is helpful to achieve monoclinic $BiVO_4$.

The percentage of the monoclinic phase in the composite-phase $BiVO_4$ has been calculated based on the normalized ration of relative intensities for the (121) peak of monoclinic phase against that for (200) peaks of the tetragonal phase [23].

$$\eta_{mono} = \frac{I_{mono(121)}}{I_{mono(121)} + I_{tetra(200)}} \times 100\%$$

where η_{mono}, $I_{momo(121)}$, $I_{tetra(200)}$ denote the percentage of the monoclinic phase, the relative intensity of the (121) peak for the monoclinic phase and that of the (200) peak for the tetragonal phase, respectively. The relationship between pH and the calculated η_{mono} is shown in Table 2. It was found that the η_{mono} increases obviously along with the improvement of pH value, which may because of the preferential formation of monoclinic in alkalescent solution [26].

Fig. 2 shows the SEM micrographs of $BiVO_4$ with different η_{mono}. It can be seen that the morphology and size of the $BiVO_4$ particles have significant changes. As shown in Fig. 2a, the pure tetragonal phase $BiVO_4$ presents a solid and smooth spherical morphology (1–3 μm), which is similar to the results reported before [17,18,23]. The morphology of mixed-phase of $BiVO_4$-b, $BiVO_4$-c and $BiVO_4$-d is mainly orbicular (1–2 μm), containing some flake form (1–3 μm). The spherical particles (1–2 μm) were gradually reduced while the flake particles (0.3–1 μm) increased gradually with the enhancement of η_{mono} (seen in Fig. 2b–d). At the same time, spherical particles and flake granules begin to link together and the two phases interweave together to form a petal-like structure with reticulate framework when η_{mono} reaches over 60% (Fig. 2d, e). Also, the surface defect appeared in surface regions of it. The possible formation mechanism is illustrated in Scheme 1. With the increase of monoclinic phase, the surface environment of $BiVO_4$ changed, and the two phase linked together to achieve the stable status. In Fig. 3f, tetragonal particles and monoclinic particles clustered into a layered structure when the content of monoclinic type $BiVO_4$ arrives at 92.73%. Interestingly, the pure monoclinic $BiVO_4$ particles (Fig. 2g) obtained at pH = 8.5 take on filmy sheet (0.05 × 0.3 μm), which is similar but quite smaller than that of traditional hydrothermal products because of its lower synthetic temperature [27–29], indicating that this synthetic route was advantageous to reduce the particles agglomeration.

Table 2
The percentage of monoclinic $BiVO_4$ (η_{mono}), BET surface areas, bandgaps (E_g), equilibrium adsorption rate of MB before irradiation and the total decolorize rate (D) after 120 min irradiation.

Item	Sample						
	(a)	(b)	(c)	(d)	(e)	(f)	(g)
η_{mono} (%)	0	10.21	34.67	66.51	72.75	92.73	100
A_{BET} ($m^2\ g^{-1}$)	1.09	1.22	2.05	3.37	3.57	4.98	7.95
E_g (eV)	2.67	2.64	2.60	2.38	2.37	2.34	2.36
Absorption rate (%)	22.0	17.8	26.0	32.5	25.4	26.2	34.1
D (%) = $(C_0 - C)/C_0 \times 100\%$	48.1	50.3	57.3	93.1	92.1	94.7	90.9

The UV–Vis diffuse reflectance spectra of the obtained samples are shown in Fig. 3. As shown in Fig. 3A, all samples exhibit absorption in the visible range in addition to the UV range. The absorption edges of samples shift to the larger wave number with the increase of η_{mono} from 500 nm to 560 nm, especially for the $BiVO_4$-f (η_{mono} = 92.73%) which shows higher visible light absorption than pure monoclinic $BiVO_4$. The steep shape of the spectra indicated that the visible-light absorption was due to the band gap transition [26].

The band gap (E_g, eV) was determined from the equation of $(\alpha h\nu)^2 = A(h\nu - E_g)^n$, in which the α, $h\nu$, A, and E_g represent absorption coefficient, incident photon energy, constant, and band gap, respectively. In the case of $BiVO_4$, the n value is 1, indicating that it is a direct band gap material [27]. The band gap energies were exhibited in Table 2. It can be seen that the E_g values of these hybrid-phase $BiVO_4$ ranged from 2.34 eV to 2.67 eV, which were consistent with the data reported previously [28,29]. But it decreased along with the increase of η_{mono}, and the least band gap reached to 2.34 eV when the η_{mono} = 92.73% in $BiVO_4$-f, which is slightly less than the band gap of pure monoclinic $BiVO_4$-g (2.36 eV). This optical behavior will play an important role in their latter photocatalytic property.

The obtained $BiVO_4$ had different specific surface areas, which are summarized in Table 2. In general, the specific BET surface area of as-synthesized $BiVO_4$ with different η_{mono} changed in the sequence of pure monoclinic $BiVO_4$ (7.95 $m^2\ g^{-1}$) > hybrid-phase $BiVO_4$ > pure tetragonal $BiVO_4$(1.09 $m^2\ g^{-1}$), which may result from its different spatial structure since the monoclinic phase is flake like and has layered structure, while the tetragonal phase presents solid orbicular form. The former may have more active absorption of site for N_2 than the latter. Besides, the BET surface area increased a little along with the increase of η_{mono} in the hybrid-phase $BiVO_4$ because of its unique reticulate framework. Obviously, the framework, specific area and surface defect are beneficial for the comprehensive performance in improving the photocatalytic activity of $BiVO_4$ [27,30,31].

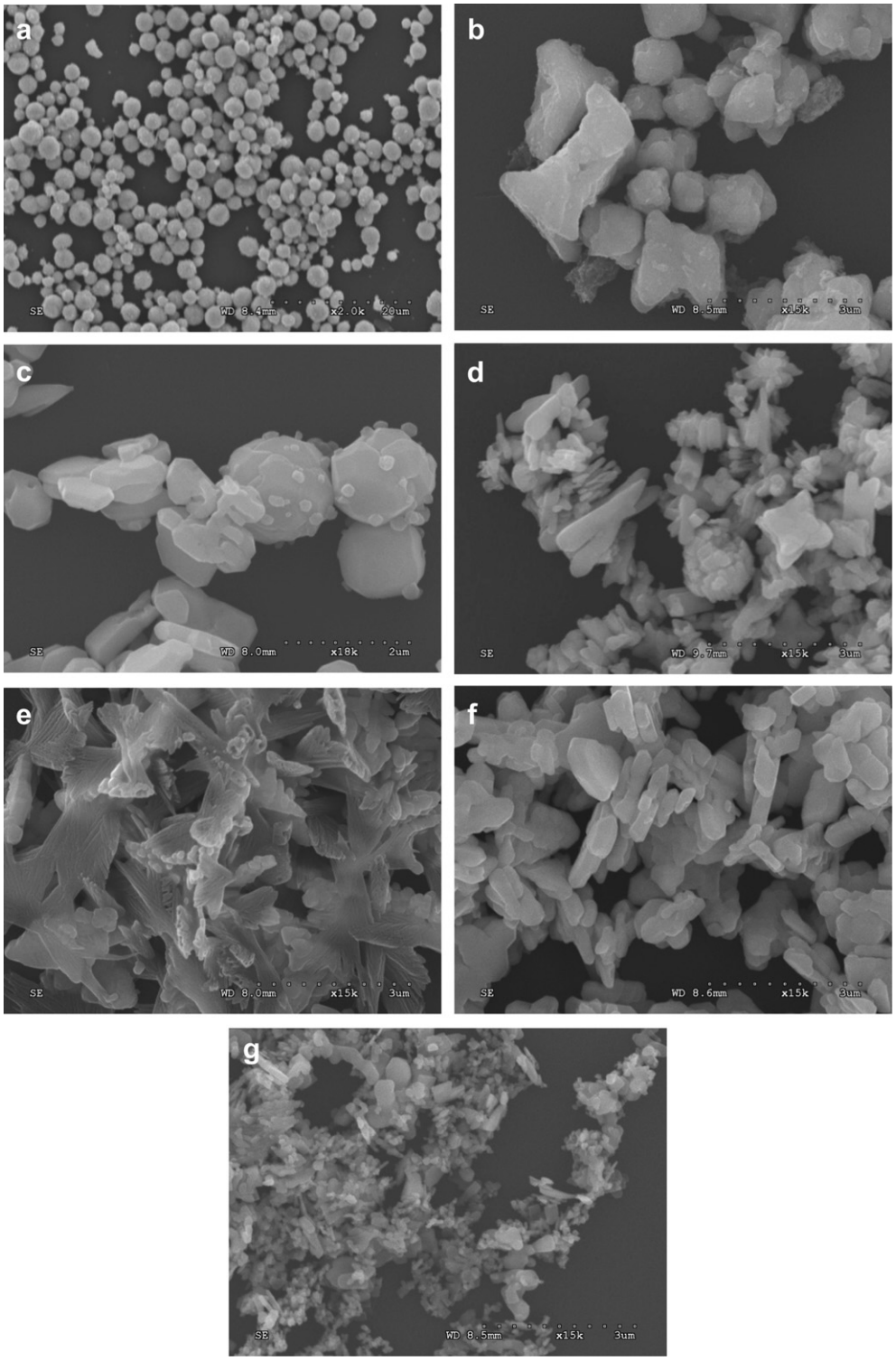

Fig. 2. SEM images of $BiVO_4$ with different η_{mono} (a) $\eta_{mono} = 0$, (b) $\eta_{mono} = 10.21\%$, (c) $\eta_{mono} = 34.37\%$, (d) $\eta_{mono} = 66.51\%$, (e) $\eta_{mono} = 72.75\%$, (f) $\eta_{mono} = 92.73\%$, (g) $\eta_{mono} = 1$.

3.2. Adsorption/photocatalytic properties of as-synthesized $BiVO_4$

To study the adsorption and photocatalytic activities of these $BiVO_4$ products, methylene blue (MB), with a major absorption band at 664 nm, was chosen as a model pollutant. It is well known that the adsorption ability of the reactant on the catalyst surface is an important factor influencing photocatalytic performance. The adsorption rates of the MB over all samples are shown in Table 2. After stirring for 30 min in darkness to reach the adsorption–desorption equilibrium, the absorption rate was 22.0% and 34.1% for the pure tetragonal $BiVO_4$ and the monoclinic $BiVO_4$ respectively, which may be accounted for the different amount active absorption site of $BiVO_4$. When associated with the BET results, we calculated the absorption capacity for per unit area in pure

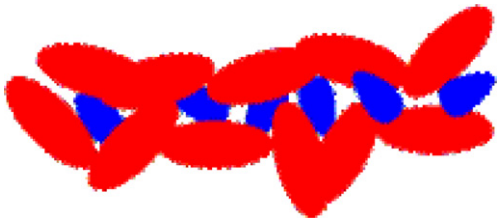

Scheme 1. The sketch map of crosslink structure with tetragonal $BiVO_4$ ( ) and monoclinic $BiVO_4$ ( ).

tetragonal $BiVO_4$-1 (2.02 mg m^{-2}), and found that it was higher than that of pure monoclinic $BiVO_4$-g (0.43 mg m^{-2}), indicating the adsorptive affinity of tetragonal $BiVO_4$ for MB is higher than that of monoclinic $BiVO_4$. Therefore, the adsorptive ability of MB dye was not only related to the surface areas of catalyst, but also related to the crystal structure of catalyst. Accordingly, although the surface area of $BiVO_4$-e sample was estimated to be 3.37 m^2 g^{-1}, the absorption rate was up to 32.5%, which was close to $BiVO_4$-g. This is very helpful for a photocatalyst in the latter photodegradation reaction.

Fig. 4 shows the variation of the MB absorbance as a function of irradiation time in the presence of as-fabricated $BiVO_4$-x (x = d, e, f, g). The MB absorbance decreased clearly with irradiation time and no new absorbance band was observed in the UV–Vis absorption spectrum, indicating the absolute degradation of MB molecules and no formation of intermediate product [30,31].

The corresponding plot for the photodegradation rate of different samples is shown in Fig. 5. The plot of the maximum

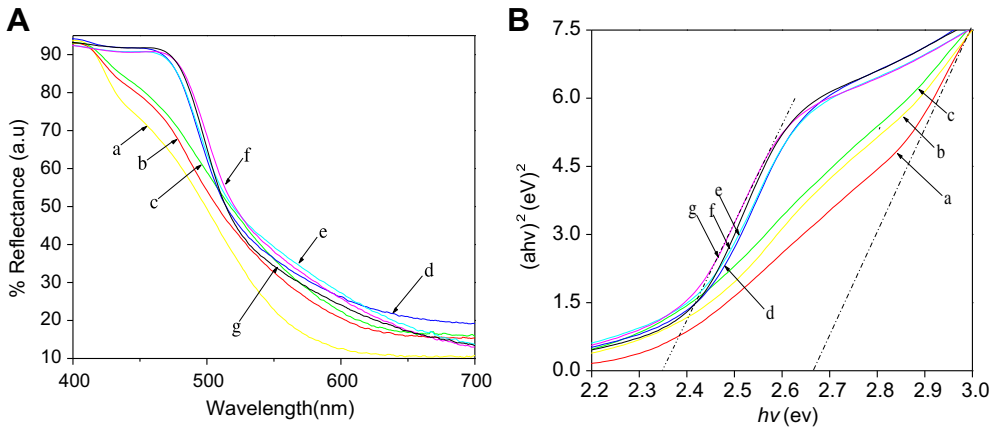

Fig. 3. (A) UV–vis diffuse reflectance spectra and (B) plots of the $(\alpha hv)^2$ versus hv of the (a) $BiVO_4$-a, (b) $BiVO_4$-b, (c) $BiVO_4$-c, (d) $BiVO_4$-d, (e) $BiVO_4$-e, (f) $BiVO_4$-f, (g) $BiVO_4$-g.

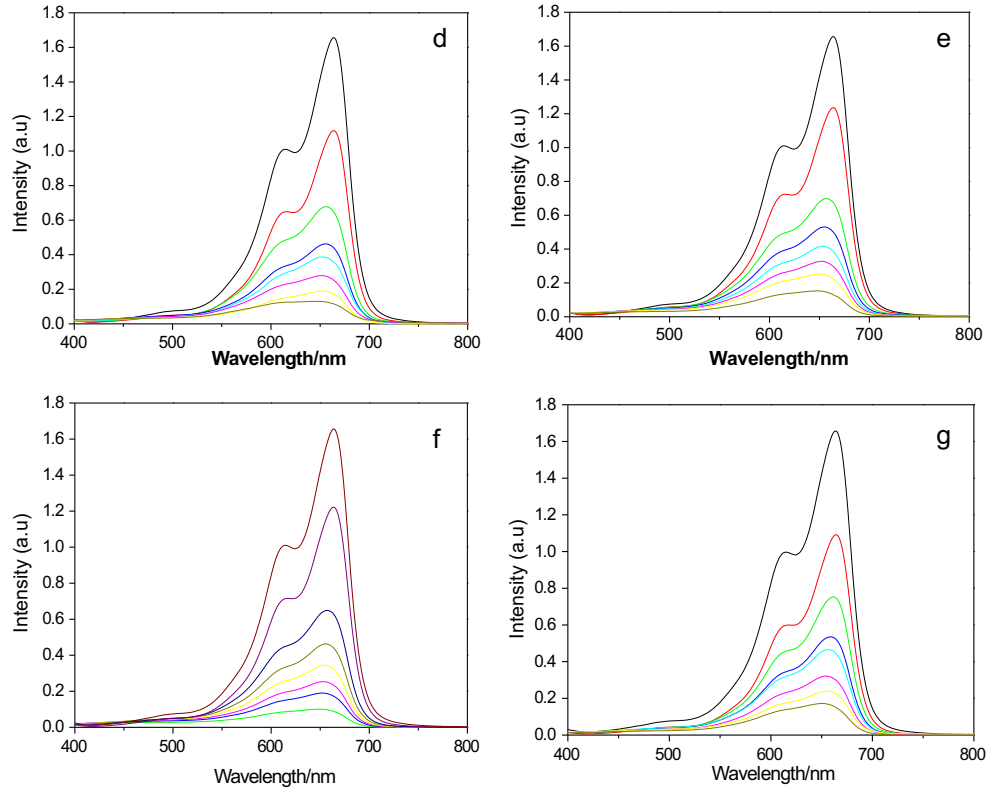

Fig. 4. UV–visible spectral changes of MB (10 mg L^{-1}) as a function of irradiation time for different photocatalysts under visible-light illumination.

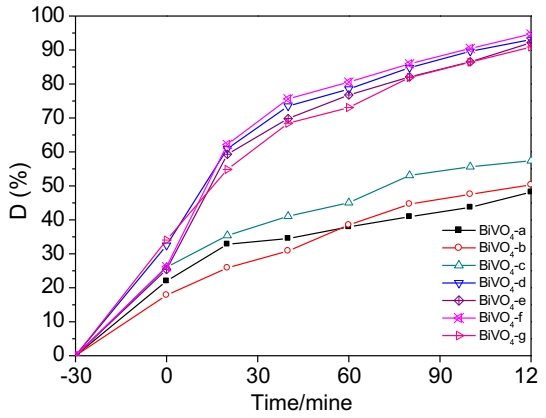

Fig. 5. Photocatalytic activities of the $BiVO_4$-x (x = a–g) for the degradation of MB under visible-light irradiation.

absorbance versus irradiation time is linear, indicating the photocatalysis reaction is a first-order reaction. Among all the $BiVO_4$-x (x = a–g) samples, the $BiVO_4$-d, $BiVO_4$-e, $BiVO_4$-f, and $BiVO_4$-g showed similar and excellent photocatalytic activity, the total decolorization rate (including absorption and photodegradation) of MB reached up to 93.1%, 92.1%, 94.7% and 90.9% after 120 min irradiation. It is generally believed that the absorption band is a fundamental immanent factor of photocatalysts. As revealed in the UV–vis spectrum, all the $BiVO_4$-x (x = d–g) samples have good response to visible light, especially for the $BiVO_4$-f.

Moreover, the efficient separation and transport of light-induced electrons and holes would account for it. For the mixed-phase $BiVO_4$-x (x = d, e), it has lower adsorptive ability and larger band gap, but it presents much higher activities than that of $BiVO_4$-g (see Fig. 5). The enhanced photocatalytic activity can be modeled on the efficient electron transfer in the inner of composite photocatalyst as shown in Scheme 2. When the tetragonal $BiVO_4$ was interwoven with monoclinic crystallites, the tetragonal $BiVO_4$ particles can act as electron traps, which promotes the electron–hole separation and subsequently transfer the trapped electron to electron acceptor (O_2 or OH^-) on the surface of the $BiVO_4$. Then the oxidative species O_2^- or ·OH were formed and the MB molecules were decomposed, while the holes still remain in the valence band of $BiVO_4$, which was similar to the novel metal doped catalysts from previous reports [32,33]. Therefore, the proximity of tetragonal particles to monoclinic particles serves to scavenge monoclinic electrons and preventing rapid recombination and stabilizing the charge separation.

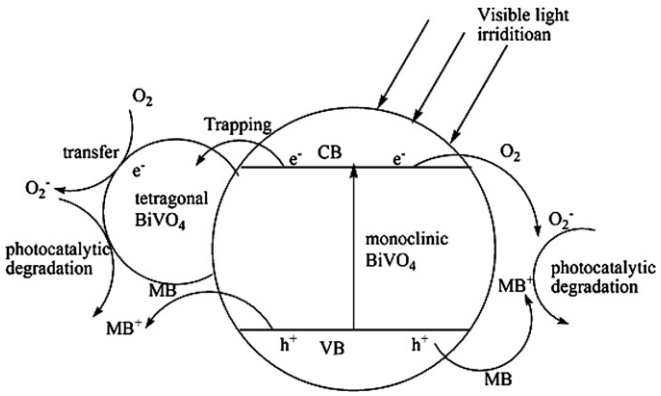

Scheme 2. Photocatalytic mechanism of mixed-phase $BiVO_4$.

4. Conclusions

Series of composite-phase $BiVO_4$ with different morphology were controlling synthesized by a facile hydrothermal method, in which the pH value of the reaction solution is playing an important role. Photocatalytic evaluation of MB revealed that hybrid-phase $BiVO_4$ presented higher photocatalytic performance than that of pure phase $BiVO_4$. From the data we have gathered, these mixed-phase $BiVO_4$ exhibiting greater photo-efficiency was due to three factors: (1) the smaller band gap of catalysts extends the useful range into the visible region; (2) the better adsorption ability of the organic compounds helps to improve the external reaction content; (3) the stabilization of charge separation by electron transfer from tetragonal particles to monoclinic particles helps to slow down the recombination of light-induced electrons and holes.

Acknowledgments

The authors thank the Program for Jiangsu Higher Institutions Key Basic Research Projects of Natural Science (10KJA430005), Natural Science Foundation of Jiangsu Province (BK2010289), Technological Research Foundation of Huai'an City (HAG2011008) and Jiangsu Government Scholarship for Overseas Studies for financial support.

References

[1] A. Mills, R.H. Davies, D. Worsley, Chem. Soc. Rev. 22 (1993) 417.
[2] K. Maeda, K. Domen, Chem. Mater. 22 (2010) 612.
[3] X.D. Tang, H.Q. Ye, Z. Zhao, H. Liu, C.X. Ma, Catal. Lett. 133 (2009) 362.
[4] H.G. Yang, C.H. Sun, S.Z. Qiao, J. Zou, G. Liu, S.C. Smith, H.M. Cheng, G.Q. Lu, Nature 453 (2008) 638.
[5] L.L. Zhang, F.J. Lv, W.G. Zhang, R.Q. Li, H. Zhong, Y.J. Zhao, Y. Zhang, X. Wang, J. Hazard. Mater. 171 (2009) 294.
[6] D. Liu, B.B. Garcia, Q.F. Zhang, Q. Guo, Y.H. Zhang, S. Sepehri, G.Z. Cao, Adv. Funct. Mater. 19 (2009) 1015.
[7] R. Asshi, T. Morikawa, T. Ohwaki, K. Aoki, Y. Taga, Science 293 (2001) 269.
[8] H.J. Zhang, G.H. Chen, D.W. Bahnemann, J. Mater. Chem. 19 (2009) 5089.
[9] Y. Li, W. Wang, X.F. Qiu, L.S., H.M. Meyer, M.P. Paranthaman, G. Eres, Z.Y. Zhang, B.H. Gu, Appl. Catal. B 110 (2011) 148.
[10] D. Chatterjee, S. Dasgupta, J. Photochem. Photobiol. C 6 (2005) 186.
[11] A. Walsh, Y. Yan, M.N. Huda, M.M.A. Jassim, S.H. Wei, Chem. Mater. 21 (2009) 547.
[12] Y.K. Kho, W.Y. Teoh, A. Iwase, L. Mädler, A. Kudo, R. Amal, Appl. Mater. Interf. 3 (2011) 1997.
[13] M. Oshikiri, M. Boero, J. Phys. Chem. B 110 (2006) 9188.
[14] J.Z. Su, L.J. Guo, N.Z. Bao, C.A. Grimes, Nano Lett. 11 (2011) 1928.
[15] A. Iwase, A. Kudo, J. Mater. Chem. 20 (2010) 7536.
[16] H.M. Fan, T.F. Jiang, H.Y. Li, D.J. Wang, L.L. Wang, J.L. Zhai, D.Q. He, P. Wang, T.F. Xie, J. Phys. Chem. C 116 (2012) 2425.
[17] G.C. Xi, J.H. Ye, Chem. Commun. 46 (2010) 1893.
[18] Y. Zhao, Y. Xie, X. Zhu, S. Yan, S.X. Wang, Chem. Eur. J. 14 (2008) 1601.
[19] J.F. Ye, W. Liu, J.G. Cai, S. Chen, X.W. Zhao, H.H. Zhou, L.M. Qi, J. Am. Chem. Soc. 133 (2011) 933.
[20] D.C. Hurum, K.A. Gray, T. Rajh, J. Phys. Chem. B 109 (2005) 977.
[21] T. Ohno, K. Sarukawa, K. Tokieda, M. Matsumura, J. Catal. 203 (2001) 82.
[22] S.W. Liu, J.G. Yu, M. Jaroniec, J. Am. Chem. Soc. 132 (2010) 11914.
[23] A.P. Zhang, J.Z. Zhang, N.Y. Cui, X.Y. Tie, Y.W. An, L.J. Li, J. Mol. Catal. A: Chem. 304 (2009) 28.
[24] J.X. Long, L.L. Zhang, S.Y. Zhou, Y.J. Zhao, C. Yao, X. Wang, J. Mater. Sci. Eng. 30 (2012) 600.
[25] L.L. Zhang, J.X. Long, W.G. Zhang, S.Y. Zhou, Y.J. Zhao, X. Wang, Chinese Creative Patent, Open number: 201110233655.X.
[26] L. Zhou, W. Wang, L. Zhang, H. Xu, W. Zhu, J. Phys. Chem. C 111 (2007) 13659.
[27] M.W. Stoltzfus, P.M. Woodward, R. Seshadri, J.H. Klepeis, B. Bursten, Inorg. Chem. 46 (2007) 3839.
[28] S.M. Sun, W.Z. Wang, L. Zhou, H.L. Xu, Ind. Eng. Chem. Res. 48 (2009) 1735.
[29] J.Q. Yu, A. Kudo, Chem. Lett. 34 (2005) 850.
[30] K. Sayama, A. Nomura, T. Arai, T. Sugita, R. Abe, M. Yanagida, T. Oi, Y. Iwasaki, Y. Abe, H. Sugihara, J. Phys. Chem. B 110 (2006) 11352.
[31] S.P. Berglund, D.W. Flaherty, N.T. Hahn, A.J. Bard, C.B. Mullins, J. Phys. Chem. C 115 (2011) 3794.
[32] A. Pandikumar, R. Ramaraj, J. Hazard. Mater. 205 (2012) 294.
[33] X.F. Zhang, X. Quan, S. Chen, Y.B. Zhang, J. Hazard. Mater. 177 (2010) 914.